Supplementary Information for

Measuring Microtubule Supertwist and Defects by Three-Dimensional-Force-Clamp Tracking of Single Kinesin-1 Motors

Michael Bugiel[†], Aniruddha Mitra[‡,¶], Salvatore Girardo[§], Stefan Diez[‡,¶], and Erik Schäffer[*,†]

[†]Cellular Nanoscience, Eberhard Karls Universität Tübingen, ZMBP, Auf der Morgenstelle 32, 72076 Tübingen, Germany.
[‡]Technische Universität Dresden, B CUBE – Center for Molecular Bioengineering and Center for Advancing Electronics Dresden, Arnoldstrasse 18, 01307 Dresden, Germany.
[¶]Max Planck Institute of Molecular Cell Biology and Genetics, Pfotenhauerstrasse 108, 01307 Dresden, Germany.
[§]Technische Universität Dresden, Center for Molecular and Cellular Bioengineering, Fetscherstraße 105, 01307 Dresden, Germany.
Corresponding author: [*]E-mail: erik.schaeffer@uni-tuebingen.de Phone: +49 7071 2978831. Fax: +49 7071 295042

Contents

List of Figures

S1. Trap fidelity

To ensure a high precision and accuracy of tracking in particular in the vertical z-direction, the trapping laser power needs to be very stable. The z-position was calculated from the sum signal of the quadrant photo diode detector by subtracting an offset voltage that corresponds to the center position. Since the sum signal and offset for the z-direction are typically 10–100× larger compared to their difference, it is essential that the laser power has low fluctuations.[1] Fluctuations of the laser power are directly proportional to the sum signal and thus cause apparent displacements in z that are not related to actual displacements. Our setup was equipped with a laser stabilization system that was able to keep fluctuations of the laser intensity below 0.003 % over 1000 s.[2] For a typical experiment, the sum signal was $V_{\mathrm{sum}} = 126\,\mathrm{mV}$ with an axial displacement sensitivity of $\beta_z = 23\,\mathrm{nm/mV}$ at the surface. A laser fluctuation of 0.003 % would then result in an apparent axial displacement of $\Delta z = 3 \cdot 10^{-5} V_{\mathrm{sum}} \beta_z \approx 0.1\,\mathrm{nm}$. In contrast, a 1 % power fluctuation would result in about 30 nm of movement demonstrating the need for a stable laser. Apart from the stable laser and trapping objective temperature, the room temperature varied by less than 0.1 °C over a 2 hour period.

During the feedback-based force-clamp tracking, the trap position was changed over a range of up to 7 µm using the piezo tilt mirror and/or piezo translation stage. Important parameters like the calibration factors should not change significantly over that range. Otherwise, the feedback would have to account for any systematic variations. Consequently, we measured displacement sensitivity and trap stiffness as a function of both the lateral and axial trap position by steering the laser focus with the piezo mirror and moving the sample with the piezo stage, respectively. These control measurements were done in a sample with surface structures at a position comparable to later experiments. The dependence of the calibration factors on the lateral trap position is shown in Fig. S1a and b. The dependence was consistent with previously reported results on flat, unstructured glass substrates.[3] Interestingly, according to parabolic fits, the displacement sensitivity and trap stiffness in the lateral directions x and y had a minimum and maximum approximately at the non-steered zero position, respectively. The corresponding relative deviations in units of %/µm are given in Fig. S1. They were calculated as differences between the minimal and maximal value normalized by the value at the zero position and the difference in position between the two values. The absolute values varied by $\lesssim$1 %/µm. Thus, even if the laser focus was moved over a range of 5 µm, the overall deviations were $\lesssim$5 %. The dependence of the calibration factors on the axial trap position is shown in Fig. S1c and d. As described by Schäffer *et al.*,[1] the calibration factors depend on the height of the microsphere above the surface. The 3D experiments were centered around a distance of ≈1.4 µm above the surface defined as the zero position. The relative deviations in the calibration factors were calculated from linear fits normalized by the zero-position value. The variation of parameters was larger than for the lateral trap positions. While for the lateral directions, the deviations were $\lesssim$4 %/µm, deviations for the axial direction were $\lesssim$13 %/µm.

S2. Micropatterned glass coverslip fabrication

A micropatterned glass coverslip was fabricated using a master generated by photolithography. In detail, a 4" silicon wafer was spin-coated with SU8 3025 photoresist diluted in SU-8 2000 thinner (1:2 w/w dilution; 3800 rpm for 30 s, acceleration 300 rpm/s) and then exposed to UV light (100 mJ/cm^2) through a chromium photomask using a mask aligner (EVG 620). Afterwards, the exposed substrate was immersed in the development solution for 5 min to remove the resist that was not irradiated by light. Subsequently, the sample was dried with nitrogen. The final master contained two different regions

DOI: 10.1021/acs.nanolett.7b04971
Nano Lett. 2018

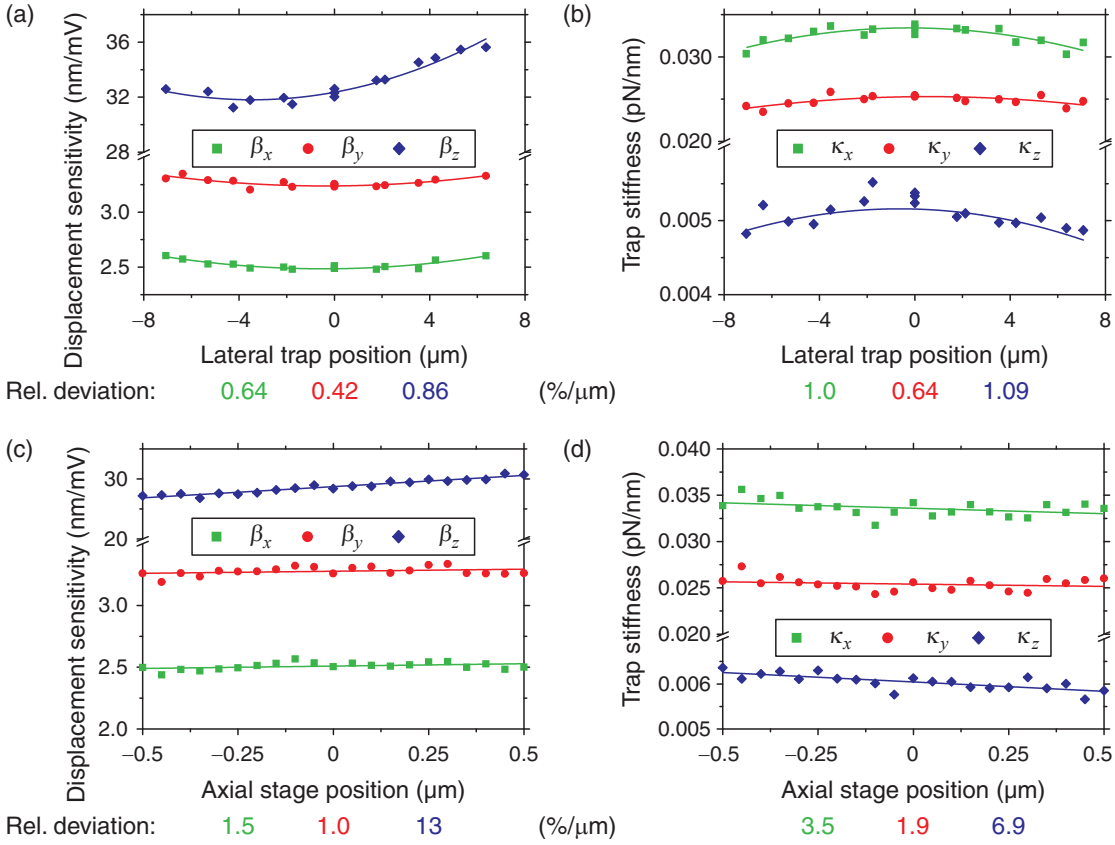

Figure S1. Dependence of the calibration factors on the lateral and axial trap position. (a) Displacement sensitivity β and (b) trap stiffness κ for a 590 nm-polystyrene microsphere as a function of the lateral trap position for the x, y, and z direction. The lateral trap position was controlled by changing the beam steering angle using a piezo tilt mirror. The solid lines are parabolic fits shown as guides to the eye. (c) Displacement sensitivity and (d) trap stiffness as a function of the axial stage position for the x, y, and z direction. Varying this piezo stage position changes the sample height and axial trap position. The solid lines are linear fits. The relative deviations for x, y, and z in percent per μm in absolute values are given below the graphs.

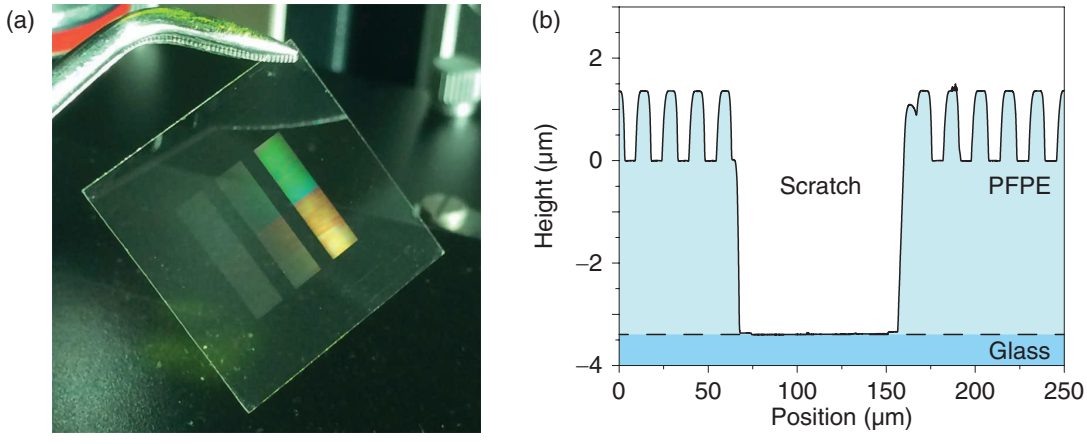

Figure S2. Micropatterned glass coverslip. (a) Picture of a patterned coverslip. The patterned coverslip has two different regions characterized by parallel grooves with a height of 1.4 μm and a width of 2 μm and 5 μm, respectively, separated by 10 μm. (b) PFPE residual and layer thickness measured with a profilometer.

DOI: 10.1021/acs.nanolett.7b04971
Nano Lett. 2018

characterized by 1.4 µm high parallel ridges with a width of 10 µm and separated by 2 and 5 µm, respectively. The patterned coverslip was then realized by a vacuum and pressure assisted replica molding process on a UV curable polymer. A mixture of perfluoropolyether (PFPE, Fluorolink MD700) and 2 % (w/w) cross-linker (Irgacure 2022) was prepared and degassed before use. The silicon master was spin-coated with an anti-sticking layer to prevent polymer adhesion during the replica molding process. A glass coverslip ($22\times22\,\mathrm{mm}^2$, thickness 150 µm) was spin-coated with KBM primer to improve the adhesion of the PFPE layer on its surface (MD700, ASL and KBM primer provided by EV group, St. Florian/Inn, Austria). The coverslip was loaded in the mask aligner, aligned and put in contact with the master. Vacuum was applied between the master and the stamp holder. In this manner, the master was pressed against the coverslip with a pressure of 1 bar reducing the thickness of the polymer residual layer after printing. The pressure defined the thickness of the residual. To polymerize PFPE, the system was exposed to UV light ($4500\,\mathrm{mJ/cm}^2$). The final patterned coverslip was then peeled off featuring the negative replica of the master (Fig. S2a). The surface topography of the patterned coverslip was characterized by a step height analysis with a profilometer equipped with a 2 µm tip. The thickness of the PFPE residual layer was measured relative to a scratch made on the PFPE surface, giving a value of about 3.4 µm (Fig. S2b).

S3. 3D-force-clamp assays

Sample chambers were built by constructing flow channels using stripes of parafilm and micropatterned coverslips. We used taxol-stabilized microtubules (4.8 mg/ml porcine tubulin, 1 mM GTP, 4 mM $MgCl_2$, and 4.8 % DMSO in BRB80 (80 mM PIPES/KOH pH = 6.9, 1 mM $MgCl_2$, 1 mM EGTA), incubated for 1.5 h at 37 °C, diluted in BRB80T (BRB80 with 10 µM taxol) and spun down in a Beckman Airfuge with 100,000 g). If not noted otherwise, all chemicals are from Sigma. Microtubules were resuspended in BRB80T and suspended over valleys by immobilization on the hydrophobic PFPE structures via tubulin antibodies (Fig. 1a). The rest of the surface was blocked from unspecific interactions by Pluronic® F-127, following standard procedures with established protocols.[4,5] We used a truncated rat kinesin-1 *rkin430* tagged with the green fluorescent protein (GFP).[6] Motors were bound specifically to 590 nm-diameter polystyrene microspheres via anti-GFP and a flexible polyethylene glycol (PEG) linker.[7] Kinesin-1-coated microspheres, diluted in motility solution (BRB80T with 0.1 mg/ml casein, 5 or 10 µM Mg-ATP, 0.1 % Tween-20, and an anti-fade cocktail containing 10 mM DTT, 20 mM glucose, 20 µg/ml glucose oxidase, 8 µg/ml catalase), were flushed into the flow cell channel. Such kinesin-1-coated microspheres were trapped and placed on suspended microtubules to await kinesin-1-initiated motility as illustrated in Fig. 1. Single-molecule conditions were achieved by reducing the kinesin-to-microsphere ratio in the solution to a value for which only one out of three microspheres showed motility following Poisson statistics.[7,8] In a second series of experiments, we reduced the PIPES concentration in the motility solution to 20 mM, as lower salt concentrations increase the processivity, i.e. the mean run length, of kinesin-1.[9,10] This buffer is denoted as BRB20. Traces from assays with BRB20 and BRB80 with a minimum duration of 2 s were analyzed together.

S4. Motor speed and run length

In 5 µM ATP and BRB80, kinesin-1 walked along microtubules with a mean speed of $94\pm5\,\mathrm{nm/s}$ ($N = 65$, SEM) and in 10 µM ATP with $187\pm5\,\mathrm{nm/s}$ ($N = 76$). In BRB20 and 5 µM ATP, the mean speed was reduced to $54\pm2\,\mathrm{nm/s}$ ($N = 132$). The values in BRB80 are consistent with velocities measured at the same ATP concentrations in total internal reflection fluorescence (TIRF) microscopy stepping assays. The mean run lengths and SEMs were 0.74 ± 0.07 µm ($N = 101$) in BRB80 and 1.1 ± 0.1µm ($N = 65$) in BRB20. Both mean values correspond to lower bounds especially for BRB20 as longer walking events were limited by the lateral working range of the force clamp of 3.5 µm from the center in each direction.

S5. Coordinate system for tracking

The lateral and vertical directions were defined as x, y, and z with the microtubule oriented along the x-axis (Fig. 1a). To align the corresponding microtubule orientation to this coordinate system, the raw 3D position data were rotated in the xy and xz-plane. The angular position ϕ (Fig. 1b) of the kinesin-1 motor on the microtubule was calculated by a circular fit to the microsphere's position in the yz-plane by

$$\phi = \mathrm{atan}\left(\frac{z-z_c}{y-y_c}\right), \tag{1}$$

where y_c and z_c are the circle's center coordinates corresponding to the position of the microtubule. An increase or decrease in ϕ corresponds to left- or right-handed rotations, respectively. The same notation is used for the supertwist pitch P. Pitches and reciprocal pitches of helical motion were calculated from the slope of a linear fit to the angular trace ϕ as a function of the forward position x according to

$$P = \frac{360\,\mathrm{deg}}{\partial\phi/\partial x}. \tag{2}$$

Previous measurements of microtubule supertwists showed that "non-supertwisted" microtubules have experimental pitches as long as several tens of micrometers.[11] Therefore, absolute pitches larger than 10 µm were denoted as non-supertwisted. Often, several traces were recorded on the same microtubule. In those cases, calculated inverse pitches were averaged to calculate one pitch value for one microtubule. The expected mean radius of the circular fit is about 350 nm corresponding to the sum of the microsphere radius (295 nm), the microtubule radius (12.5 nm[12]), and the length of the kinesin-1/PEG linker of about 40 nm.[5] This value was used for circular fits, when the angular trace was not long or helical enough to determine the radius by a fit. The somewhat larger measured radius (see main text) may be due to fluctuations of the microtubule. The radial position ρ with respect to the fitted radius was calculated by

$$\rho = \sqrt{(z-z_c)^2+(y-y_c)^2}. \tag{3}$$

The mean of this radial position corresponded to the fitted radius. The position signals were recorded with 4 kHz and smoothed with a running median filter over 500 data points for all further analysis.

S6. Gliding Assays

As a control, we performed gliding assays with kinesin-1 and speckled microtubules as described before.[14] Speckled

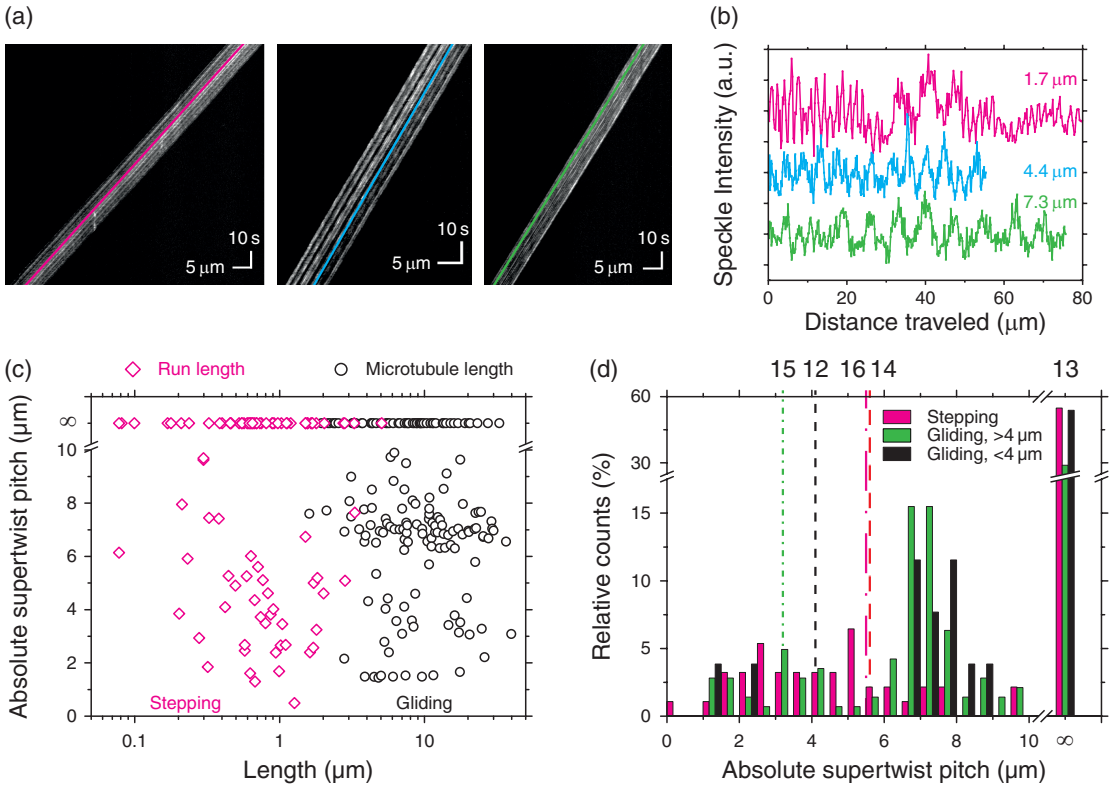

Figure S3. Gliding assays with kinesin-1 and speckled microtubules. (a) Three exemplary kymographs (space-time intensity plots) of speckled microtubules driven by kinesin-1. Individual speckles showed periodic intensity variations, corresponding to the speckles' height. (b) Intensity profiles along the lines in the kymographs in (a) revealing oscillations. Corresponding rotational pitches are given. (c) Absolute pitches of both gliding and stepping assays as a function of microtubule and run length, respectively. (d) Histogram of absolute pitches of both gliding and stepping assays. Vertical lines indicate expected values for absolute pitches[13] of supertwisted microtubules with 12–16 protofilaments. For gliding assays, histograms are shown for microtubules that were shorter and longer than 4 µm.

microtubules contain tubulin clusters with a higher rhodamine labeling ratio that are brighter than the surrounding lattice. Gliding assays using those microtubules were performed on silicon wafers coated with full-length kinesin-1[15] and imaged using fluorescence interference contrast (FLIC) microscopy. Flow cells were built out of wafers and coated with casein and kinesin-1 as described before.[15] Afterwards, motility solution of the same composition as for the optical tweezers assays (except for tween-20) together with speckled microtubules were flushed in. Taxol-stabilized rhodamine-speckled microtubules were grown similarly to microtubules used in the 3D-force-clamp assays using a 1:30 mixture of rhodamine-labeled and unlabeled tubulin. Microtubule rotations were measured by tracking the height-dependent intensity of localized speckles of rhodamine-labeled tubulin in the microtubule lattice using FLIC as shown in Fig. S3a. Rotational pitches were calculated by power spectral density analysis of the position-dependent intensity signal (Fig. S3b). The gliding assays confirmed microtubule rotations with a comparable range of pitches as in the optical tweezers stepping assays (Fig. S3c and d). However, the handedness of the rotation could not be determined with this method. Therefore, we plotted absolute pitches. Motors in stepping and gliding assays interacted with different proportions of microtubule lengths (Fig. S3c). Stepping assays probed only short sections of microtubules limited by the kinesin-1 run length. Gliding assays averaged pitches over the whole length of the microtubule. Furthermore, the influence of changes in the protofilament number of a microtubule in a gliding assay could not be observed directly. To test whether switches in protofilament numbers, expected to occur on average every 4 µm, led to a microtubule length dependence of pitches in gliding assays, we plotted histograms of pitches for microtubules that were shorter or longer than 4 µm (Fig. S3d). We observed nearly twice as many straight microtubules having 13 protofilaments for short compared to long microtubules when probed by gliding assays (about 55 % vs. 30 %; note the break in the scale of the relative counts). This larger percentage of straight microtubules was consistent with the stepping assays. For longer microtubules, the number of straight microtubules was reduced because gliding assays averaged over straight and supertwisted sections. This averaging procedure most likely led to larger pitch values of the gliding assays compared to the stepping assays.

DOI: 10.1021/acs.nanolett.7b04971
Nano Lett. 2018

S7. Applying Loads to Motors Walking on Freely Suspended Microtubules

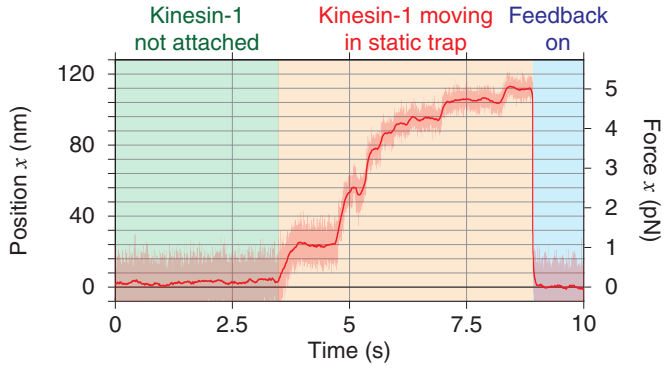

Figure S4. Position and force as a function of time of a motor-coated microsphere on a freely suspended microtubule. With opposing loads in a static trap, the kinesin-1 stalled at ≈5 pN prior to engaging the 3D-force clamp with a zero load. Individual motor steps can be discerned.

References

(1) Schäffer, E., Nørrelykke, S. F. & Howard, J. Surface forces and drag coefficients of microspheres near a plane surface measured with optical tweezers. *Langmuir* **23**, 3654–3665 (2007).

(2) Mahamdeh, M. & Schäffer, E. Optical tweezers with millikelvin precision of temperature-controlled objectives and base-pair resolution. *Opt. Express* **17**, 17190–17199 (2009).

(3) Bugiel, M., Jannasch, A. & Schäffer, E. Implementation and tuning of an optical tweezers force-clamp feedback system. In Gennerich, A. (ed.) *Optical Tweezers: Methods and Protocols*, chap. 5 (Springer Press, 2017).

(4) Jannasch, A., Bormuth, V., Storch, M., Howard, J. & Schäffer, E. Kinesin-8 is a low-force motor protein with a weakly bound slip state. *Biophys. J.* **104**, 2456–2464 (2013).

(5) Bugiel, M., Böhl, E. & Schäffer, E. The kinesin-8, kip3, switches microtubule protofilaments in a sideward random walk asymmetrically biased by force. *Biophys. J.* **108**, 2019–27 (2015).

(6) Rogers, K. R. *et al.* Kif1d is a fast non-processive kinesin that demonstrates novel k-loop-dependent mechanochemistry. *EMBO J.* **20**, 5101–5113 (2001).

(7) Bugiel, M. *et al.* Versatile microsphere attachment of gfp-labeled motors and other tagged proteins with preserved functionality. *JBM* **2**, e30 (2015).

(8) Block, S. M., Goldstein, L. S. B. & Schnapp, B. J. Bead movement by single kinesin molecules studied with optical tweezers. *Nature* **348**, 348–352 (1990).

(9) Vale, R. D. *et al.* Direct observation of single kinesin molecules moving along microtubules. *Nature* **380**, 451–453 (1996).

(10) Thorn, K. S., Ubersax, J. A. & Vale, R. D. Engineering the processive run length of the kinesin motor. *J. Cell Biol.* **151**, 1093–1100 (2000).

(11) Ray, S., Meyhöfer, E., Milligan, R. A. & Howard, J. Kinesin follows the microtubule's protofilament axis. *J. Cell Biol.* **121**, 1083–1093 (1993).

(12) Howard, J. *Motor Proteins and the Cytoskeleton* (Sinauer Associates, Sunderland, MA, 2001).

(13) Wade, R. & Chrétien, D. Cryoelectron microscopy of microtubules. *J. Struct. Biol.* **110**, 1–27 (1993).

(14) Mitra, A., Ruhnow, F., Nitzsche, B. & Diez, S. Impact-free measurement of microtubule rotations on kinesin and cytoplasmic-dynein coated surfaces. *PLOS ONE* **10**, e0136920 (2015).

(15) Korten, T., Chaudhuri, S., Tavkin, E., Braun, M. & Diez, S. Kinesin-1 expressed in insect cells improves microtubule in vitro gliding performance, long-term stability and guiding efficiency in nanostructures. *IEEE Trans. Nanobioscience* **15**, 62–69 (2016).